Open Journal of Physical Chemistry, 2011, 1, 28-36
doi:10.4236/ojpc.2011.12005 Published Online August 2011 (http://www.SciRP.org/journal/ojpc)

Photocatalytic Degradation of 4-Chlorophenol by $CuMoO_4$-Doped TiO_2 Nanoparticles Synthesized by Chemical Route

Tanmay K. Ghorai*
Department of Chemistry, *West Bengal State University*, *Barasat*, *Kolkata*, *India*
E-mail: *tanmay_ghorai@yahoo.co.in
Received April 23, 2011; *revised May* 29, 2011; *accepted July* 7, 2011

Abstract

The photocatalytic degradation of 4-chlorophenol (4-CP) in aqueous solution was studied using $CuMoO_4$-doped TiO_2 nanoparticles under Visible light radiation. The photocatalysts were synthesized by chemical route from TiO_2 with different concentration of $CuMoO_4$ ($Cu_xMo_xTi_{1-x}O_6$; where, x values ranged from 0.05 to 0.5). The prepared nanoparticles are characterized by XRD, BET surface area, TEM, UV-vis diffuse reflectance spectra, Raman spectroscopy, XPS and EDAX spectroscopy were used to investigate the nanoparticles structure, size distribution, and qualitative elemental analysis of the composition. The $Cu_xMo_xTi_{1-x}O_6$ (x = 0.05) showed high activity for degradation of 4-CP under visible light. The surface area of the catalyst was found to be 101 m^2/g. The photodegradation process was optimized by using $Cu_xMo_xTi_{1-x}O_6$ (x = 0.05) catalyst at a concentration level of 1 g/l. A maximum photocatalytic efficiency of 96.9% was reached at pH = 9 after irradiation for 3 hours. Parameters affecting the photocatalytic process such as catalyst loading, concentration of the catalyst and the dopant concentration, solution pH, and concentration of 4-CP have been investigated.

Keywords: Inorganic Compounds, Chemical Synthesis, Nanostructures, Optical Properties

1. Introduction

The photocatalytic degradation of different toxic compounds such as organic or inorganic pollutants, eliminated through photochemical reaction by using TiO_2 photocatalysts, has been widely studied [1-8]. It is an attractive technique for the complete destruction of undesirable contaminants in both liquid and gaseous phase by using artificial light of solar illumination [9].

There are so many techniques used for the complete annihilation of undesirable contaminants in both liquid and gaseous phase by using artificial light and nano photocatalyst TiO_2 [10-12]. However, there are two serious limitations, which were found in the conventional TiO_2 catalyst system that limits its practical applications. First, setting velocity of aggregated TiO_2 (average diameter of 0.2 μm) is very slow, thus requiring a long retention time in the clarifier. Second, as the quantity of TiO_2 is increased in order to increase the photocatalytic rate, the high turbidity created by the high TiO_2 concentration can decrease the depth of UV penetration. This effect can drastically lower the rate of photocatalytic reaction on a unit TiO_2 weight basis. Therefore the applications for metal ions have been used for doping TiO_2 [13-16] to increase the photocatalytic property by influencing generation and recombination of the charge carriers under light. Barkat et al and Woo et al reported that photodegradation of 2-chlorophenol by Co-doped TiO_2 and 4-chlorophenol by Ni^{2+}-doped TiO_2 were photoactive under UV light but they did not investigate the degradation of 2/4-chlorophenol with P25 TiO_2 [17-18]. The effects of copper (II) ions have been studied on the photodegradation of the insecticide monocrophos [19], photocatalytic degradation of sucrose [20], acetic acid [21], phenol [22], and methyl orange [23]. But there is no such example of copper molybdenum doped TiO_2 photocatalysts. A successful application of $CuMoO_4$-doped TiO_2 is the easy degradation of 4-chlorophenol in aqueous medium in presence of UV light. It is of interest to know how the photocatalytic degradation induced by TiO_2 doped metal ions will affect the treatment of water. The dopant ions or oxides can also modify the band gap

or act as change separators of the photoinduced electron-hole pair thus enhancing the photocatalytic activity [24].

In this paper, we report the preparation of copper molybdenum doped TiO_2 nano photocatalyst by chemical solution decomposition methods. The photocatalytic activities of the synthesized copper molybdenum doped TiO_2 nanocatalysts were compared with P 25 titania by examining the photodegradation of 4-CP as a model photocatalytic reaction under visible light. The $Cu_xMo_xTi_{1-x}O_6$ (x = 0.05) (CMT1) shows better photocatalytic activity compared to P25 TiO_2 and the other compositions of copper molybdate doped titanium dioxide $Cu_xMo_xTi_{1-x}O_6$ (x = 0.1) (CMT2), $Cu_xMo_xTi_{1-x}O_6$ (x = 0.5) (CMT3) photocatalyst for photodegradation of 4-CP.

2. Experimental Section

2.1. Synthesis of Nanosized Anatase $CuMoO_4$-Doped TiO_2

The total synthesis was carried out in two steps by chemical solution decomposition method (CSD). In the first step the stock of $Cu(NO_3)_2{\cdot}6H_2O$ (Aldrich, 99.99%), $(NH_4)_2MoO_4$ (Aldrich, 99.99%) and titanium tartarate solutions were prepared. The titanium tartarate solution was prepared by the following procedure. TiO_2 powder (Aldrich, 99.99%) is dissolved in 40% HF solution in a 500 ml teflon beaker kept on an water bath for ~24 h. During warming on the water bath, the solution was shaken occasionally. The clear fluoro complex of titanium was then precipitated with 25% NH_4OH solution. The precipitate was filtered and thoroughly washed with 5% aqueous solution of NH_4OH to make the precipitate fluoride free. Then the hydroxide precipitate of titanium is dissolved in tartaric acid (Aldrich, 99.99%) solution. The strength of the Ti^{4+} in titanium tartarate solution was estimated by gravimetric method.

In the second step, the equivalent amount of copper nitrate, ammonium molybdate, and titanium tartarate solution were taken in a beaker as per chemical composition. The complexing agent TEA (triethanolamine) (MERCK, Mumbai, India) (where molecular ratio of metal ion:TEA = 1:3) was added to the homogeneous solution of constituents maintaining pH at 6 - 7 by nitric acid (65%) and ammonia. The mixed solution was dried at 200˚C, resulting in a black carbonaceous light porous mass which was calcinated at three different temperatures namely 500˚C, 600˚C and 700˚C for 2 h at a heating rate of 5˚C/min for different chemical compositions of $Cu_xMo_xTi_{1-x}O_6$ (x = 0.05, 0.1, 0.5) nano powders. Complete synthesis procedure is presented below in the **Flowchart 1** diagram.

2.2. Photocatalytic Activity

The photocatalytic activities of the newly prepared nanosized $Cu_xMo_xTi_{1-x}O_6$ (x = 0.05, 0.1, 0.5) powders were characterized using photodegradation of 4-chlorophenol to carbon dioxide and water in aerated aqueous solution as a model photoreaction. The photocatalytic reactions were carried out by slow stirring the mixture using a magnetic stirrer with simultaneous irradiation by visible light source using a 300-W Xe lamp with a cut off filter (λ > 420 nm). The reactions were performed by adding nano powder of each photocatalyst (0.1 g) and the concentration of 4-CP is 50 ppm, into each set of a 100 ml of different solution of 4-CP. However, the efficiency of photodegradation of 4-CP is maximum at 10 ppm in the presence of prepared catalyst. The system was thoroughly repeated by several cycles of evacuation.

A small volume (1ml) of reactant liquid was siphoned out at regular interval of time for analysis. It was then centrifuged at 1500 rpm for 15 min, filtered through a 0.2 μm-millipore filter to remove the suspended catalyst particles and analyzed for the residual concentration of 4-CP by high performance liquid chromatograph (HPLC). The efficiency of the decolorization process at pH = 9 is measured by the following Equation (1), as a function of time.

$$\text{Efficency} = 100 \times \frac{(C_0 - C)}{C_0} \quad (1)$$

Here C_0 and C are the initial and remaining 4-CP concentrations in the solution, respectively.

2.3. Characterization

The crystallinity of the prepared nano powders was checked by powder X-ray diffraction (XRD) with a Rigaku Model Dmax 2000 diffractometer using CuKa radiation (λ = 1.54056 Å) at 50 kV and 150 mA by scanning at 2˚ 2θ min^{-1}. Scherer's equation was applied using the (101) peak to determine the pseudo-average particle size of nanosized anatase $CuMoO_4$ doped TiO_2 to reveal the effects of the preparation parameters on the crystal growth: $D = K\lambda/(\beta\cos\theta)$, where K was taken as 0.9, and β is the full width of the diffraction line at half of the maximum intensity.

The energy dispersive X-ray spectroscopy (EDX) (JEOL JMS-5800) was used to study the qualitative elemental analysis and element localization on samples being analyzed. BET surface area measurements were carried out using a (BECKMAN COULTER SA3100) on nitrogen adsorption desorption isotherm at 77K.

The morphology and the size of TiO_2 nanocrystallites were investigated by high resolution transmission elec-

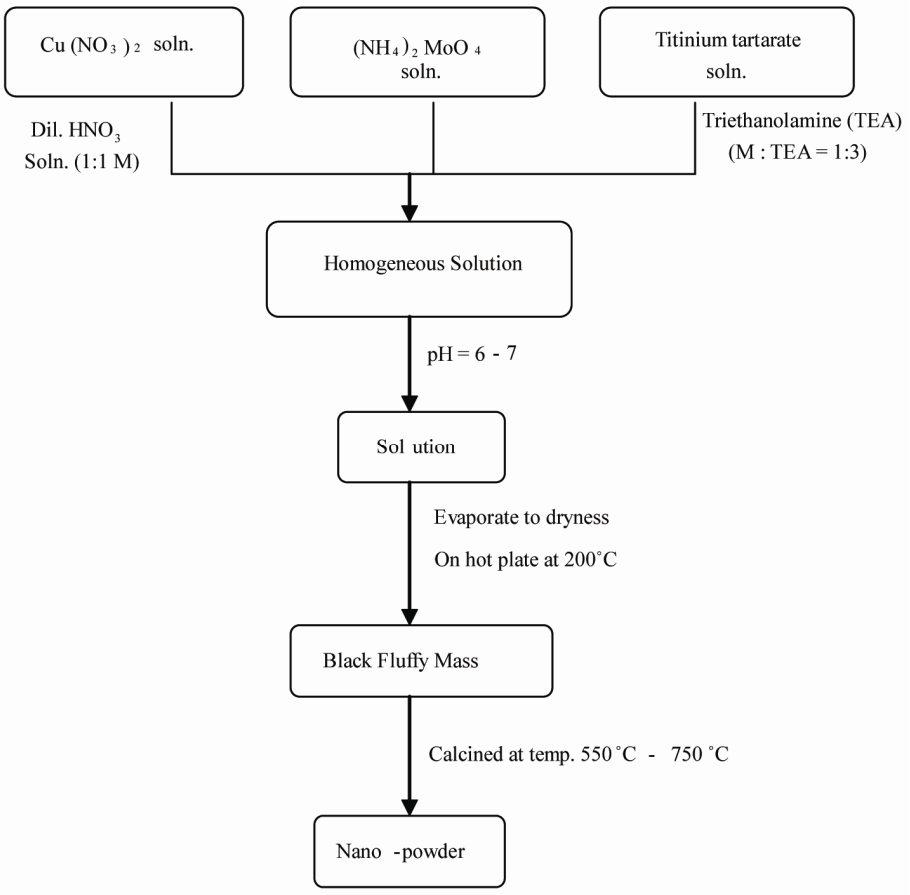

Flowchart 1. Synthesis of different composites of nanosized copper molybdenum doped titanium dioxide $Cu_xMo_xTi_{1-x}O_6$ (x = 0.05, 0.1, 0.5) photocatalysts.

tron microscopy (HRTEM) with a JEOL-2010F at 200 kV. The particle size distribution of TiO_2 nanocrystallites was determined by directly measuring the particle sizes on the TEM images. The average particle size of each sample was determined by using the size distribution data based on a weighted-averages method.

The catalytic activity of the prepared nanoparticles was measured in a batch photoreactor containing appropriate solutions of 4-CP with visible light irradiation of 300-W Xe lamp. High performance liquid chromatography (HPLC) was used for analyzing the concentration of 4-CP in solution at different time intervals during the photodegradation experiment.

Raman spectrum was obtained by using a Perkin Elmer Spectrum GX Raman instrument. The UV-vis diffuse reflectance spectra of the prepared powders were obtained by a UV-vis spectrophotometer (UV-1601 Shimadzu) at room temperature

3. Results and Discussion

3.1. XRD Analysis

The XRD pattern of copper molybdenum doped titanium dioxide, $Cu_xMo_xTi_{1-x}O_6$ [when x = 0.05 (CMT1), 0.1 (CMT2) & 0.5 (CMT3)], copper doped TiO_2 [Cu-TiO_2 (CT)] and $CuMoO_4$ (CM) are shown in **Figure 1** at 550˚C. It can be seen that the peaks at 2θ of 25.26˚, 38.16˚, 48.17˚, 54.03˚, 55.12˚, and 64.69˚ are assigned to (101), (004), (200), (105), (211), and (204) respectively (JCPDS data File No. 84 1285) lattice planes of TiO_2, which are attributed to the signals of anatase phase. No additional peaks were found to be present, which could be assigned to the $CuMoO_4$ anorthic phase that indicated that the resulting nano powder was alloy of copper molybdate with titanium dioxide. Rutile phase was not observed for all specimens using different Ti precursors. The XRD patterns of $Cu_xMo_xTi_{1-x}O_6$ (x = 0.05) recorded at room temperature after annealing the samples at various temperatures, indicated no change of crystallographic characteristics shown in **Figure 2**. Furthermore, the EDAX spectroscopy measurements (**Figure 3**) show a molar ratio of $CuMoO_4$: TiO_2 equal to about 0.05:0.95.

3.2. Transmission Electron Microscopy (TEM) Study

Bright field TEM (Model JEOL-2010F) micrograph of

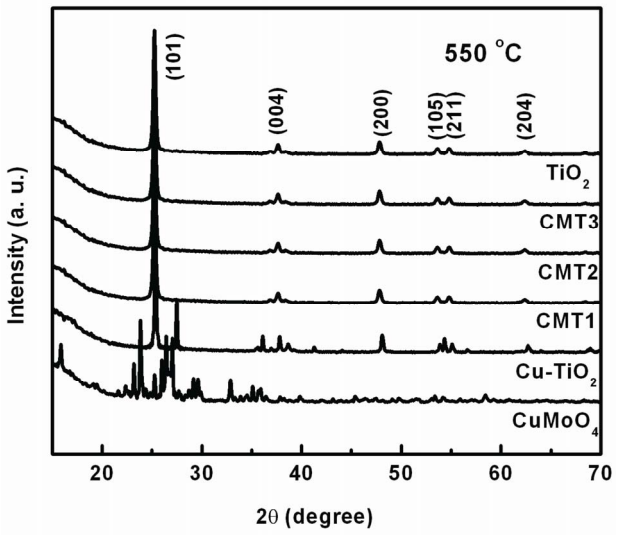

Figure 1. XRD patterns of $CuMoO_4$ (CM), copper doped TiO_2 (CT), copper molybdenum doped titanium dioxide (CMT1, CMT2, CMT3), and TiO_2 photocatalyst at 550˚C.

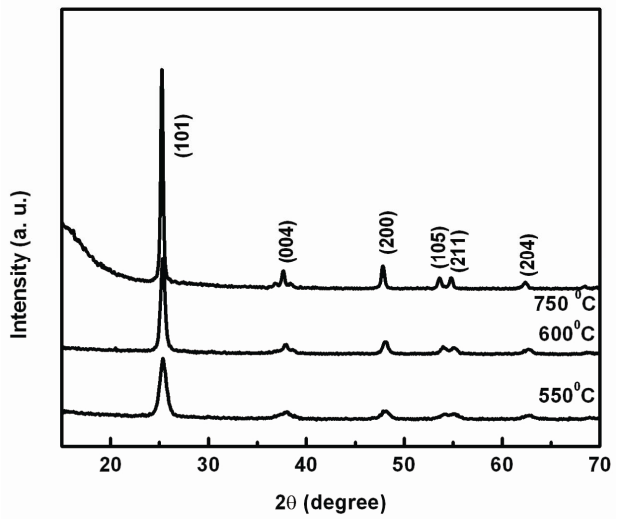

Figure 2. XRD of $Cu_xMo_xTi_{1-x}O_6$ (x = 0.05) recorded at room temperature after annealing the samples at various temperatures.

$Cu_xMo_xTi_{1-x}O_6$ (x = 0.05) (CMT1) nanoparticles is presented in **Figure 4**. The fine particles are spherical, of narrow size distribution and have an average particle size of about 10 ± 2 nm analyzed by soft ware Image Tool. However, the average crystallite size of CMT determined by the peak broadening method was found to be about 12 - 13 nm obtained from XRD analysis (shown in **Table 1**). The corresponding selected area electron diffraction pattern of the same sample (CMT1) showed distinct rings, characteristic of a single crystalline nanoparticle as shown in **Figure 4** (inset).

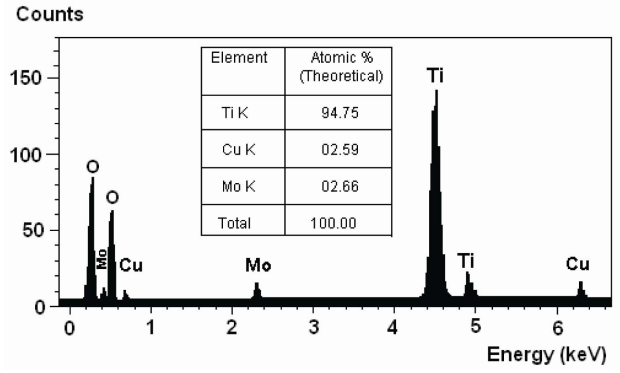

Figure 3. EDAX of $Cu_xMo_xTi_{1-x}O_6$ (x = 0.05).

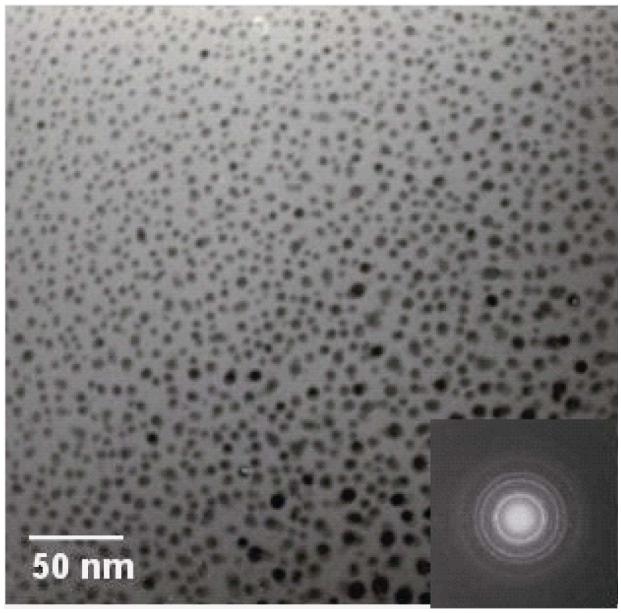

Figure 4. Bright field TEM micrograph and selected area electron diffraction (SAED) (inset) pattern of sample CMT1.

Table 1. Resultant properties of CMT1, CMT2, CMT3, P25 TiO_2, CM and CT composites.

Sample	Photodegradation Efficiency (%)	S_{BET} (m^2/g)	Anatase Crystal size (nm)	Bandgap Energy (eV)
CMT1	96.9	101	11.89	3.03
CMT2	87.8	92	12.52	3.09
CMT3	58.7	92	11.97	3.12
CM	38.2	50	24.21	3.15
CT	25.2	32	14.49	2.82
P25 TiO_2	11.2	49	12.42	3.29

Photodegradation efficiency; BET surface area measured by dinitrogen adsorption desorption isotherm at 550˚C; Anatase crystal size calculated from Scherer equation.

3.3. Specific Surface Area (BET) Analysis

The BET of different compositions of CMT1, CMT2, CMT3, P25 TiO_2, CM and CT calcined at 550˚C temperatures is listed in **Table 1**, which is measured by dini-

trogen adsorption-desorption isotherm in BECKMAN COULTER SA3100. It is noted that BET decreases as dopant concentration of metal ions increases at a particular composition. The sample CMT1 having high specific surface area, which was about 101 ± 5 m^2/g, provided good photocatalytic properties among all the photocatalysts against 4-CP. Hence the large surface area enhanced photocatalytic activity through efficient adsorption of the reactant on the catalyst surface.

3.4. Raman Spectroscopy

Raman analysis of $CuMoO_4$-doped TiO_2 alloy may allow us to rationalize these results. The Raman spectra of prepared nanoparticles calcined at 550˚C with varying mol% of $CuMoO_4$ in TiO_2 is shown in **Figure 5.** The analysis of Raman bands suggests that all active materials having bands at 337 cm^{-1} for CuO_2 [25] in-plane bond-bending mode and 971 cm^{-1} for Mo [26] correspond to Mo = O bond stretching modes. Except the above two bands, all the mentioned bands matched with characteristic bands of titania.

3.5. XPS Analysis

Figure 6 shows the results of XPS spectra of $Cu_xMo_xTi_{1-x}O_6$ (x = 0.05). $CuMoO_4$ doped TiO_2 where the concentration of $CuMoO_4$ is 0.05 mole, the Cu_2O/CuO and MoO_3 are shown in **Figure 6** to identify the copper and molybdenum state on the surface of TiO_2. The Cu (2p)- binding energies of Cu_2O/CuO were found to be 932.8 and 953.4 eV, respectively and corresponding Mo (2p)- binding energy is 233.0 eV. According to the position and the shape of the peaks, the copper on the surface of TiO_2 may exist in multiple-oxidation states. Oxygen and Ti show surface characteristic photoelectron peaks. **Figure**

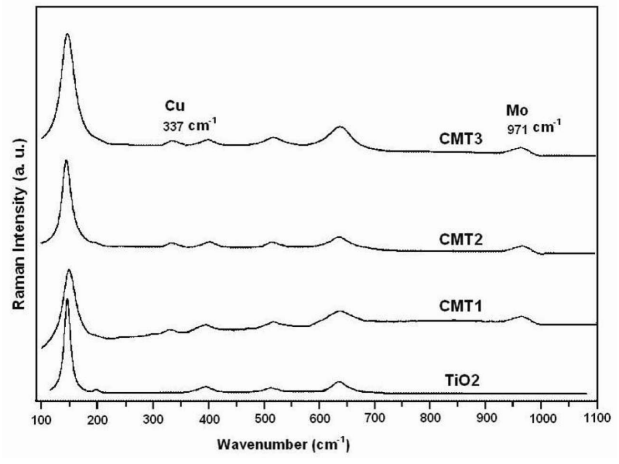

Figure 5. Raman spectra of CMT1, CMT2, CMT3 and TiO_2.

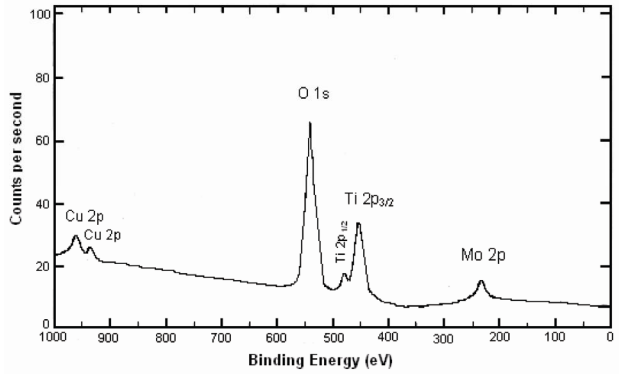

Figure 6. XPS of $Cu_xMo_xTi_{1-x}O_6$ (x = 0.05).

shows the binding energy of O (1s) at 533.4 eV and Ti (2p) at 454.9 eV ($2p_{3/2}$) and 461.3 eV ($2p_{1/2}$) corresponding to Oxygen and Ti metal.

3.6. UV-VIS Diffuse Reflectance Spectrum

The UV-vis diffuse reflectance spectrum and band gap energy of all the compositions are shown in **Figure 7** and **Table 1** respectively. From **Figure 7** and **Table 1** we may conclude that the UV-vis diffuse reflectance spectrum of CuMoO4 doped TiO2 and pure TiO2, gave distinct band gap absorption edges at 409 nm, 401 nm, 397 nm and 387 nm for doped CMT1, CMT2, CMT3 and pure TiO2 and corresponding band gap energies are 3.03, 3.09, 3.12 and 3.20 eV respectively. At lowest concentration of $CuMoO_4$, the absorption edge shift is maximum hence the corresponding calculated band gap energy is minimum. This is explained considering that when the amount of dopants is small, the metals ions are well incorporated into the lattice withstanding the

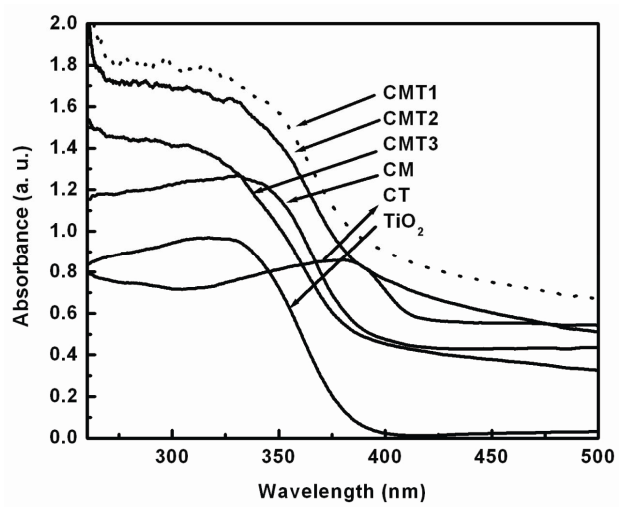

Figure 7. The UV-visible diffuse reflectance spectra of M-Ti samples with the highest dopant-atom content.

evolvement of local strains. On the other hand, when the dopants are in excess, $CuMoO_4$ cannot enter the TiO_2 lattice but cover on the surface of TiO_2 in MO_3 form, and leads to the formation of heterogeneity junction. So, $Cu_xMo_xTi_{1-x}O_6$ (x = 0.05) photocatalysts has lower band gap energy (3.03 eV) highest within the temperature range in which the experiments were carried out photocatalytic activity compared to other dopant concentrations and P25 TiO_2.

3.7. Photocatalytic Activity of the Prepared Samples

The evaluation of the efficiency of photodegradation of 4-CP as a function of different experimental parameters is demonstrated in **Figures 8-11**. To study the effect of the catalyst on the 4-CP photodegradation rates, samples are annealed at different calcinations temperatures. The activities strongly depended on the calcination temperature of the catalysts. **Figure 8** summarizes the results of these experiments. The highest degradation of 4-CP was achieved with samples that were annealed at 550˚C. However, increase in the calcinations temperatures of the catalysts decrease the photocatalytic activity due to increase of particle size and decrease of the specific surface area. The crystalline nature of the anatase structure is primarily responsible for the photocatalytic activity of the nanoparticles. Particles with anatase structure are known to have a better photocatalytic activity [27]. Moreover, the small particle size of CMT1 (about ~10 nm) provides a large surface area where the catalytic reactions could occur and the photoreactivity is enhanced.

The effect of the dopant concentration on the photocatalytic activity of different compositions of copper molybdate doped titanium dioxide photocatalyst, on photodegradation of 4-CP has been presented in **Figure 9**. From **Figure 9**, it could be noted that the dopant concentration in TiO_2 has a great impact upon its photocatalytic activity to decolorize 4-CP solution at pH = 9. The photodegradation efficiency of 4-CP decreased with increasing $CuMoO_4$ concentration, reaching a maximum value of 96.9% with sample containing 0.05 mol% $CuMoO_4$ that was annealed at 550˚C. The photodegradation efficiency of 4-CP using all the photocatalyst are presented in **Table 1**. The anatase CMT1 nanocrystallites with regular crystal surfaces should have less surface defects, giving highly efficient photocatalysis by suppression of electron-hole pair recombination through redox cycle between Cu(II) and Cu(I). Cu(II) ions work as electrons scavengers which may react with the superoxide species and prevent the holes-electrons (h^+/e^-) recombination and consequently increase the efficiency of the photo-oxidation. The possible reaction is shown below:

$$Cu(II) + O_2^-{}_{(ads)} = Cu(I) + O_{2(ads)} \quad (2)$$

Defect sites are identified as Ti^{3+} on the TiO_2 surface due to adsorption and photoactivation of oxygen thus, increasing the photocatlaytic efficiency. Electron can be also excited from defect energy levels Ti^{3+}, to the TiO_2 conduction band and photodegradation occurs.

$$Ti^{3+} + O_2^- \rightarrow Ti^{+4} + O_2^- \quad (3)$$

Figure 10 shows the effect of the $CuMoO_4$-doped TiO_2 dosage on the 4-CP degradation. It can be seen that in the absence of the catalyst about 12% of 4-CP was removed at pH 9 after 3 h of irradiation of UV. This is

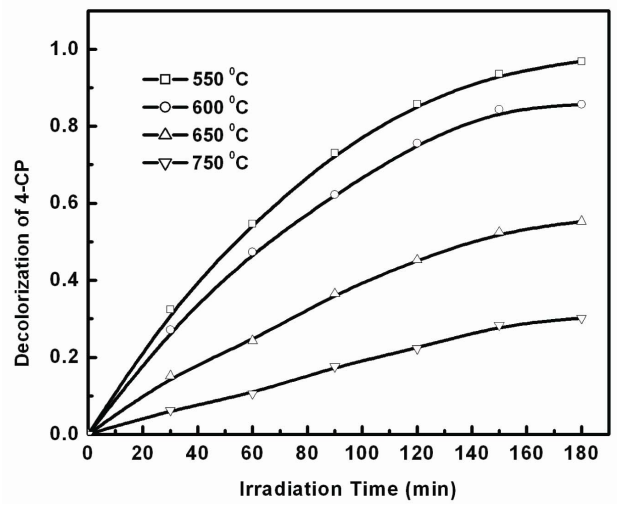

Figure 8. Photocatalytic effect of the CMT1 crystal structure on the 4-CP photodegradation at different calcinations temperatures.

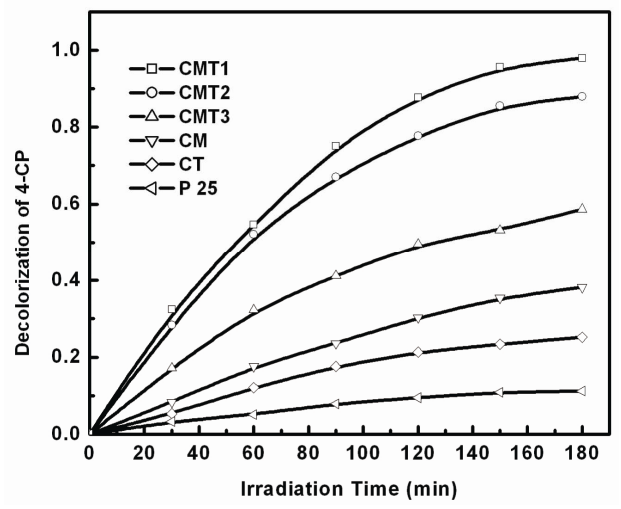

Figure 9. Photocatalytic effect of CMT1, CMT2, CMT3, P25, CM and CT on the 4-CP photodegradation. Catalyst dosage = 1 g/L, 4-CP = 50 ppm, pH = 9.

mainly a photolysis process. The degradation of 4-CP is increased by adding $CuMoO_4$ doped TiO_2 with $CuMoO_4$ concentration of 0.05 mol%. The degradation reached a maximum value of 96.9 with catalyst dosage of 1 g/L and the optimize concentration of 4-CP is 50 ppm. However, a further increase in the catalyst dosage slightly decreased the degradation efficiency. The photodecomposition rates of pollutants are influenced by the active site and the photo-absorption of the catalyst used. Adequate loading of the catalyst increases the generation rate of electron/hole pairs for enhancing the degradation of pollutants. However, addition of a high dose of the semiconductor decreases the light penetration by the photocatalyst suspension [28] and reduces the degradation rate. A Langmuir-Hinshelwood type [29] of relationship can be used to describe the effect of 4-CP concentration on its degradation.

The pH of the solution has a strong effect on the photodegradation process, as shown in **Figure 11**. Degradation efficiency of 4-CP has not been found to be significant at low pH values but increased rapidly with increase of the pH, attaining a maximum value of 96.9% for pH of 9. Further increase in pH of 4-CP decreases the photodegradation efficiency, because the protons are potential determining ions for TiO_2, and the surface charge development is affected by the pH [30].

Upon hydration, surface hydroxyl groups (TiOH) are formed on TiO_2. These surface hydroxyl groups can undergo proton association or dissociation reactions, thereby bringing about surface charge which is pH-dependent and photodegradation occurs.

However, the dopant concentrations of the prepared catalyst above an optimal value result in the formation of

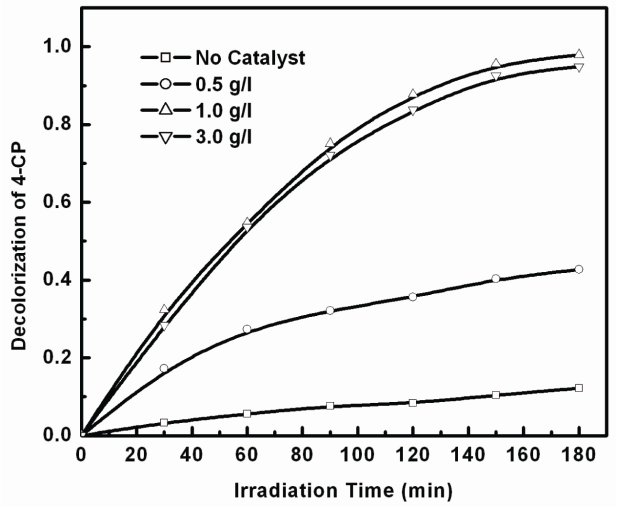

Figure 10. Effect of the $CuMoO_4$-doped TiO_2 dosage on the 4-CP photodegradation. Co = 0.036 mol%, 2-CP = 50 ppm, pH = 9.

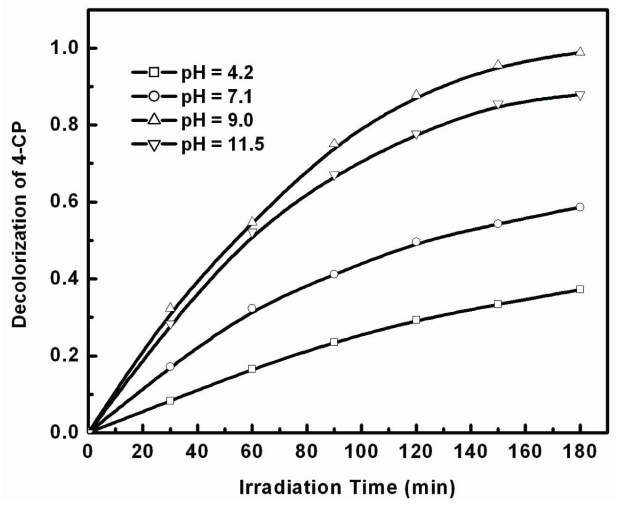

Figure 11. Photocatalytic effect of the solution pH on the 4-CP photodegradation. $CMT1_{catalyst}$ dosage = 1 g/L, 4-CP = 50 ppm.

recombination centers which traps the charges for a very long time thereby reducing the photodegradation performance.

4. Conclusions

In this study, nanophotocatalyst $CuMoO_4$ (5 mole%) doped TiO_2 synthesized by CSD method is more photoactive than all other compositions of copper molybdate doped TiO_2 and P25 TiO_2 due to high surface area (101 m^2/g), lower band-gap (3.03 eV) and photochemical degradation on 4-CP through redox cycle between Cu(II) and Cu(I). The typical composition of the prepared $CuMoO_4$ doped TiO_2 was $Cu_xMo_xTi_{1-x}O_6$ with the value of x ranging from 0.05 to 0.5. The photocatalytic activity strongly depends on $CuMoO_4$ doping concentration. The photodegradation process was optimized by using $Cu_xMo_xTi_{1-x}O_6$ (x = 0.05) catalyst at a concentration level of 1g/L. A maximum photocatalytic efficiency of 96.9% was reached at pH = 9 after irradiation for 3 hours. The light absorption measurements confirmed that the presence of 5 mol% $CuMoO_4$ doped TiO_2 structure caused significant absorption shift into the visible region compared to the pure TiO_2 powder.

5. Acknowledgements

The authors thank the Council of Scientific and Industrial Research, India, for financial support and Prof. Mukut Chakraborty for English correction of the manuscript.

6. References

[1] J. C. Yu, G. S. Li, X. C. Wang, X. L. Hu, C. W. Leung

and Z. D. Zhang, "An Ordered Cubic Im3m Mesoporous Cr-TiO_2 Visible Light Photocatalyst," *Chemical Communications*, Vol. 25, 2006, pp. 2717-2719. doi:10.1039/b603456j

[2] T. Tatsuma, S. Tachibana, T. Miwa, D. A. Tryk and A. Fujishima, "Remote Bleaching of Methylene Blue by UV-Irradiated TiO2 in the Gas Phase," *Journal of Physical Chemistry B*, Vol. 103, No. 38, 1999, pp. 8033-8035. doi:10.1021/jp9918297

[3] S. Parra, S. E. Stanca, I. Guasaquillo and K. R. Thampi, "Photocatalytic Degradation of Atrazine Using Suspended and Supported TiO_2," *Applied Catalysis B: Environmental*, Vol. 51, No. 2, 2004, pp. 107-116. doi:10.1016/j.apcatb.2004.01.021

[4] T. Tatsuma, S. Tachibana and A. Fujishima, "Remote Oxidation of Organic Compounds by UV-Irradiated TiO2 via the Gas Phase," *Journal of Physical Chemistry B*, 2001, Vol. 105, No. 29, pp. 6987-6992. doi:10.1021/jp011108j

[5] Y. Chen, K. Wang and L. Lou, "Photodegradationof Dye Pollutants on Silica Gel Supported $Ti0_2$ Particles Undervisible Light Irradiation," *Journal of Photochemistry and Photobiology A*: *Chemistry*, Vol. 163, No. 1-2, 2004, pp. 281-287. doi:10.1016/j.jphotochem.2003.12.012

[6] K. Kawahara, Y. Ohko, T. Tatsuma and A. Fujishima, "Surface Diffusion Behavior of Photo-Generated Active Species or Holes on TiO_2 Photocatalysts," *Physical Chemistry Chemical Physics*, 2003, Vol. 5, No. 21, pp. 4764-4766. doi:10.1039/b311230f

[7] I. K. Konstantinou and T. A. Albanis, "TiO2-Assisted Photocatalytic Degradation of Azo Dyes in Aqueous Solution: Kinetic and Mechanistic Investigations," *Applied Catalysis B: Environmental*, Vol. 49, No. 1, 2004, pp. 1-14. doi:10.1016/j.apcatb.2003.11.010

[8] N. L. Wu, M. S. Lee, Z. J. Pon and J. Z. Hsu, "Effect of Calcination Atmosphere on TiO_2 Photocatalysis in Hydrogen Production from Methanol/Water Solution," *Journal of Photochemistry and Photobiology A: Chemistry*, Vol. 163, No. 1-2, 2004, pp. 277-280. doi:10.1016/j.jphotochem.2003.12.009

[9] H. Q. Zhan and H. Tian, "Photocatalytic Degradation of Acid Azo Dyes in Aqueous TiO_2 Suspension I. The Effect of Substituents," *Dyes and Pigments*, Vol. 37, No. 3, 1998, pp. 231-239. doi:10.1016/S0143-7208(97)00060-0

[10] A. Fuerte, M. D. Hernandez-Alonso, A. J. Maira, A. Martínez-Arias, M. Fernandez-Garcia, J. C. Conesa and J. Soria, "Visible Light-Activated Nanosized Doped-TiO_2 Photocatalysts," *Chemical Communications*, 2001, pp. 2718-2719. doi:10.1039/b107314a

[11] C. Adan, A. Bahamonde, M. Fernandez-Garcia and A. Martinez-Arias, "Structure and Activity of Nanosized Iron-Doped Anatase TiO_2 Catalysts for Phenol Photocatalytic Degradation," *Applied Catalysis B: Environmental*, Vol. 72, No. 1-2, 2007, pp. 11-17. doi:10.1016/j.apcatb.2006.09.018

[12] H. Yin, Y. Wada, T. Kitamura, S. Kambe, S. Murasawa, H. Mori, T. Sakata and S. Yanagida, "Hydrothermal Synthesis of Nanosized Anatase and Rutile TiO_2 Using Amorphous Phase TiO_2," *Journal of Materials Chemistry*, Vol. 11, No. 6, 2001, pp. 1694-1703. doi:10.1039/b008974p

[13] N. I. Al-Salim, S. A. Bagshaw, A. Bittar, T. Kemmitt, A. J. McQuillan, A. M. Mills and M. J. Ryan, "Characterisation and Activity of Sol-Gel Prepared TiO/sub2 Photocatalysts Modified with Ca, Sr or Ba Ion Additives," *Journal of Materials Chemistry*, Vol. 10, No. 10, 2000, pp. 2358-2363.

[14] R. Niishiro, H. Kato and A. Kudo, "Nickel and Either Tantalum or Niobium-Codoped TiO_2 and $SrTiO_3$ Photo-Catalysts with Visible-Light Response for H_2 or O_2 Evolution from Aqueous Solutions," *Physical Chemistry Chemical Physics*, Vol. 7, 2005, pp. 2241-2245. doi:10.1039/b502147b

[15] C.-Y. Wang, C. Bottcher, D. W. Bahnemann and J. K. Dohrmann, "A Comparative Study of Nanometer Sized Fe(III)-Doped TiO2 Photocatalysts: Synthesis, Characterization and Activity," *Journal of Materials Chemistry*, Vol. 13, 2003, pp. 2322-2329. doi:10.1039/b303716a

[16] M. Gratzel and F. H. Russell, "Electron Paramagnetic Resonance Studies of Doped Titanium Dioxide Colloids," *The Journal of Physical Chemistry*, Vol. 94, No. 6, 1990, pp. 2566-2572. doi:10.1021/j100369a064

[17] M. A. Barakata, H. Schaeffer, G. Hayes and S. Ismat-Shah, "Photocatalytic Degradation of 2-Chlorophenol by Co-Doped TiO_2 Nanoparticles," *Applied Catalysis B: Environmental*, Vol. 57, No. 1, 2004, pp. 23-30. doi:10.1016/j.apcatb.2004.10.001

[18] S. H. Woo, W. W. Kim, S. J. Kim and C. K. Rhee, "Photocatalytic Behaviors of Transition Metal Ion Doped TiO_2 Powder Synthesized by Mechanical Alloying," *Materials Science and Engineering: A*, Vol. 449-451, 2007, pp. 1151-1154. doi:10.1016/j.msea.2006.01.165

[19] Z. Hua, Z. Manping, X. Zongfeng and G. K.-C. Low, "Titanium Dioxide Mediated Photocatalytic Degradation of Monocrotophos ," *Water Research*, Vol. 29, No. 12, 1995, pp. 2681-2688. doi:10.1016/0043-1354(95)00141-7

[20] D. Beydoun, H. Tse, R. Amal, G. Low and S. McEvoy, "Effect of Copper(II) on the Photocatalytic Degradation of Sucrose," *Journal of Molecular Catalysis A*: *Chemical*, Vol. 177, No. 2, 2002, pp. 265-272. doi:10.1016/S1381-1169(01)00272-2

[21] M. Bideau, B. Claudel, L. Faure and H. Kazouan, "The Photo-Oxidation of Acetic Acid by Oxygen in the Presence of Titanium Dioxide and Dissolved Copper Ions," *Journal of Photochemistry and Photobiology A*: *Chemistry*, Vol. 61, No. 2, 1991, pp. 269-280. doi:10.1016/1010-6030(91)85095-X

[22] K. I. Okamoto, Y. Yamamoto, H. Tanaka, M. Tanaka and A. Itaya, "Heterogeneous Photocatalytic Decomposition of Phenol over TiO_2 Powder," *Bulletin of the Chemical Society of Japan*, Vol. 58, 1985, p. 20.

[23] T. K. Ghorai, D. Dhak, S. K. Biswas, S. Dalai and P. Pramanik, "Photocatalytic Oxidation of Organic Dyes by Nano-Sized Metal Molybdate Incorporated Titanium Dioxide ($M_xMo_xTi_{1-x}O_6$) (M = Ni, Cu, Zn) Photocatalysts,"

Journal of Molecular Catalysis A: Chemical, Vol. 237, No. 1-2, 2007, pp. 224-229. doi:10.1016/j.molcata.2007.03.075

[24] N. I. Al-salim, S. A. Bagshaw, A. Bittar, T. Kemmitt, A. J. McQuillan, A. M. Mills and M. J. Ryan, "Characterisation and Activity of Sol-Gel-Prepared TiO_2 Photocatalysts Modified with Ca, Sr or Ba Ion Additives," *Journal of Materials Chemistry*, Vol. 10, 2000, pp. 2358-2363.

[25] M. Krantz, H. J. Rosen, R. M. Macfarlane and V. Y. Lee, "Effect of Oxygen Stoichiometry on Softening of Raman Active Lattice Modes in $YBa_2Cu_3O_x$," *Physical Review B*, Vol. 38, No. 7, 1988, pp. 4992-4995. doi:10.1103/PhysRevB.38.4992

[26] I. E. Wachs, "Raman and IR Studies of Surface Metal Oxide Species on Oxide Supports: Supported Metal Oxide Catalysts," *Catalysis Today*, Vol. 27, No. 3-4, 1996, pp. 437-455. doi:10.1016/0920-5861(95)00203-0

[27] A. Doongr and W. H. Chang, "Photodegradation of Parathion in Aqueous Titanium Dioxide and Zero Valent Iron Solutions in the Presence of Hydrogen Peroxide," *Journal of Photochemistry and Photobiology A: Chemistry*, Vol. 116, No. 3, 1998, pp. 221-228. doi:10.1016/S1010-6030(98)00292-5

[28] M. A. Fox and M. T. Dulay, "Heterogeneous Photocatalysis," *Chemical Reviews*, Vol. 93, No. 1, 1993, pp. 341-357. doi:10.1021/cr00017a016

[29] D. Chen and A. K. Ray, "Photocatalytic Kinetics of Phenol and Its Derivatives over UV Irradiated TiO_2," *Applied Catalysis B: Environmental*, Vol. 23, No. 2-3, 1999, pp. 143-157. doi:10.1016/S0926-3373(99)00068-5

[30] J. M. Tseng and C. P. Huang, "Removal of Chlorophenols from Water by Photocatalytic Oxidation," *Water Science and Technology*, Vol. 23, 1991, p. 377.

